INTERNATIONAL JOURNAL FOR NUMERICAL METHODS IN FLUIDS
Int. J. Numer. Meth. Fluids 2004; **45**:751–773 (DOI: 10.1002/fld.713)

Linear and non-linear stability analysis for finite difference discretizations of high-order Boussinesq equations

David R. Fuhrman[1,*,†], Harry B. Bingham[1], Per A. Madsen[1] and Per G. Thomsen[2]

[1]*Department of Mechanical Engineering, Technical University of Denmark, DK-2800 Kgs. Lyngby, Denmark*
[2]*Informatics and Mathematical Modelling, Technical University of Denmark, DK-2800 Kgs. Lyngby, Denmark*

SUMMARY

This paper considers a method of lines stability analysis for finite difference discretizations of a recently published Boussinesq method for the study of highly non-linear and extremely dispersive water waves. The analysis demonstrates the near-equivalence of classical linear Fourier (von Neumann) techniques with matrix-based methods for formulations in both one and two horizontal dimensions. The matrix-based method is also extended to show the local de-stabilizing effects of the non-linear terms, as well as the stabilizing effects of numerical dissipation. A comparison of the relative stability of rotational and irrotational formulations in two horizontal dimensions provides evidence that the irrotational formulation has significantly better stability properties when the deep-water non-linearity is high, particularly on refined grids. Computation of matrix pseudospectra shows that the system is only moderately non-normal, suggesting that the eigenvalues are likely suitable for analysis purposes. Numerical experiments demonstrate excellent agreement with the linear analysis, and good qualitative agreement with the local non-linear analysis. The various methods of analysis combine to provide significant insight into the numerical behaviour of this rather complicated system of non-linear PDEs.

KEY WORDS: Boussinesq equations; stability analysis; local non-linear analysis; method of lines; finite differences; pseudospectra

1. INTRODUCTION

This paper considers a *method of lines* stability analysis for the recently published Boussinesq formulation of References [1, 2] for the study of highly non-linear and extremely dispersive water waves. This formulation combines exact representations of the kinematic and dynamic free surface conditions with truncated series expansion solutions (about an arbitrary vertical z-level, $\hat{z}$) of the Laplace equation and the kinematic bottom condition. Through the combined

*Corrrespondence to: D. R. Fuhrman, Department of Mechanical Engineering, Technical University of Denmark, Studentertorvet, Building 101E, DK-2800 Kgs. Lyngby, Denmark.
†E-mail: drf@mek.dtu.dk

Contract/grant sponsor: Danish Technical Research Council (STVF); contract/grant number: 9801635

Published online 19 April 2004
Received 29 June 2003
Revised 22 January 2004

use of Padé-enhanced expansions, along with the retainment of the vertical velocity w as an unknown, the resulting formulation has been shown in References [1, 2] to provide accurate linear and non-linear qualities up to (wavenumber times depth) $kh \approx 25$, and accurate velocity profiles up to $kh \approx 12$—for the first time removing any practical limitations on the relative water depth conventionally associated with Boussinesq-type approximations. A number of efficient numerical solution techniques for this system can be found in Reference [3], however issues concerning the numerical stability of such solutions have not yet been addressed, which is the aim here.

Herein, we consider the stability of a number of finite difference discretizations of the previously noted high-order Boussinesq formulation. The methods used include a classical linear Fourier (von Neumann) analysis in a single horizontal dimension, as well as a matrix-based method in two horizontal dimensions (for both rotational and irrotational formulations), with all of the analyses providing similar results. While the rotational and irrotational systems exhibit similar linear properties, experience has shown that their non-linear behaviour can be quite different. We therefore extend the matrix-based method to include the temporally local effects of the non-linear terms. As will be demonstrated, the addition of the non-linear terms tends to de-stabilize the resulting eigenvalue distributions, while numerical dissipation is demonstrated to have a stabilizing effect. A comparison of the two formulations provides clear evidence that the irrotational formulation has significantly better stability properties in highly non-linear, deep-water situations, consistent with observations. Computation of matrix pseudospectra also demonstrates that the system is only moderately non-normal (with increased eigenvalue sensitivity for the rotational formulation), giving confidence that the eigenvalues reasonably characterize the discrete systems. To confirm the results from the analysis, a series of numerical experiments are conducted using explicit fourth-order, four stage Runge–Kutta time integration. The results demonstrate excellent quantitative agreement with the linear analyses, and good qualitative agreement with the local non-linear analysis. This work serves as an example of the combined use of many widely applicable analysis techniques, with each providing significant insight into the numerical behaviour of this complicated system. This analysis has proven essential in obtaining convergent numerical solutions for this important system of non-linear partial differential equations (PDEs).

The outline of this paper is as follows. The Boussinesq formulation is outlined in Section 2. The method of lines approach for numerical stability is briefly described in Section 3. In Section 4 a classical linear Fourier (von Neumann) stability analysis is undertaken in a single horizontal dimension for two separate sets of finite difference approximations. An alternative matrix-based linear stability analysis is used in Section 5 in two horizontal dimensions, which is further extended to include the temporally local effects of the non-linear terms in Section 6. This section also demonstrates the effects of numerical dissipation on the system, and includes a comparison of rotational and irrotational formulations. Analysis of matrix pseudospectra is provided in Section 7. A series of numerical experiments with both the linear and non-linear models is detailed in Section 8. Conclusions are drawn in Section 9.

2. THE BOUSSINESQ FORMULATION

Consider the flow of an incompressible, inviscid fluid with a free surface. A Cartesian coordinate system is adopted, with the x- and y-axis located on the still-water plane, and with the

z-axis pointing vertically upwards. The fluid domain is bounded by the sea bed at $z=-h(\mathbf{x})$, with $\mathbf{x}=\langle x, y\rangle$, and the free surface at $z=\eta(\mathbf{x},t)$, where t is time. Water wave formulations commonly include exact representations of the non-linear free surface boundary conditions, expressed in terms of velocity variables at the free surface (see e.g. References [1, 2, 4]). This leads to the following expressions for the kinematic and dynamic free surface conditions (in two horizontal dimensions):

$$\frac{\partial \eta}{\partial t}=\tilde{w}\left(1+\left(\frac{\partial \eta}{\partial x}\right)^2+\left(\frac{\partial \eta}{\partial y}\right)^2\right)-\tilde{U}\frac{\partial \eta}{\partial x}-\tilde{V}\frac{\partial \eta}{\partial y}+D\nabla^2\eta \tag{1}$$

$$\frac{\partial \tilde{U}}{\partial t}=-g\frac{\partial \eta}{\partial x}-\frac{1}{2}\frac{\partial}{\partial x}\left(\tilde{U}^2+\tilde{V}^2-\tilde{w}^2\left(1+\left(\frac{\partial \eta}{\partial x}\right)^2+\left(\frac{\partial \eta}{\partial y}\right)^2\right)\right)+D\nabla^2\tilde{U} \tag{2}$$

$$\frac{\partial \tilde{V}}{\partial t}=-g\frac{\partial \eta}{\partial y}-\frac{1}{2}\frac{\partial}{\partial y}\left(\tilde{U}^2+\tilde{V}^2-\tilde{w}^2\left(1+\left(\frac{\partial \eta}{\partial x}\right)^2+\left(\frac{\partial \eta}{\partial y}\right)^2\right)\right)+D\nabla^2\tilde{V} \tag{3}$$

where

$$\tilde{\mathbf{U}}=\langle \tilde{U}, \tilde{V}\rangle=\tilde{\mathbf{u}}+\tilde{w}\nabla\eta \tag{4}$$

Here $\tilde{\mathbf{u}}=\langle \tilde{u}, \tilde{v}\rangle$ and $\tilde{w}$ are the horizontal and vertical velocities directly on the free surface (i.e. at $z=\eta$), $g=9.81\,\mathrm{m/s^2}$ is the gravitational acceleration, and $\nabla=\langle \partial/\partial x, \partial/\partial y\rangle$ is the horizontal gradient operator. Note that diffusive terms with diffusion coefficient D have been added to each of the free surface conditions. These will be used in Sections 6–8 to investigate the effects of numerical dissipation. By inspection of (1)–(4) it can be seen that evolving η and $\tilde{\mathbf{U}}$ forward in time requires a means of computing the associated $\tilde{w}$, subject to the Laplace equation and the kinematic bottom condition

$$w+\nabla h\cdot\mathbf{u}=0, \quad z=-h \tag{5}$$

This can be expressed quite generally as

$$\tilde{w}=f(\eta,\tilde{\mathbf{U}}) \tag{6}$$

Most solutions to the exact water wave problem can be expressed in this form, with different approximations for (6). In the present analysis we focus on the highly accurate Boussinesq-type method described in detail in References [1, 2] (see also Reference [5]). In this formulation the vertical distribution of fluid velocity is approximated by

$$\mathbf{u}(\mathbf{x},z,t)=(1-\alpha_2\nabla^2+\alpha_4\nabla^4)\hat{\mathbf{u}}^*(\mathbf{x},t)+((z-\hat{z})\nabla-\beta_3\nabla^3+\beta_5\nabla^5)\hat{w}^*(\mathbf{x},t) \tag{7}$$

$$w(\mathbf{x},z,t)=(1-\alpha_2\nabla^2+\alpha_4\nabla^4)\hat{w}^*(\mathbf{x},t)-((z-\hat{z})\nabla-\beta_3\nabla^3+\beta_5\nabla^5)\hat{\mathbf{u}}^*(\mathbf{x},t) \tag{8}$$

where

$$\begin{aligned}
\alpha_2&=\frac{(z-\hat{z})^2}{2}-\frac{\hat{z}^2}{18}, & \alpha_4&=\frac{(z-\hat{z})^4}{24}-\frac{\hat{z}^2(z-\hat{z})^2}{36}+\frac{\hat{z}^4}{504}\\
\beta_3&=\frac{(z-\hat{z})^3}{6}-\frac{\hat{z}^2(z-\hat{z})}{18}, & \beta_5&=\frac{(z-\hat{z})^5}{120}-\frac{\hat{z}^2(z-\hat{z})^3}{108}+\frac{\hat{z}^4(z-\hat{z})}{504}
\end{aligned} \tag{9}$$

In (7) and (8) the quantities $\hat{\mathbf{u}}^*$ and $\hat{w}^*$ are pseudo-velocity variables at an arbitrary vertical expansion point $\hat{z}$, which have been introduced to allow Padé enhancement of the Taylor series operators. Optimal velocity distributions are obtained near $\hat{z} = -h/2$, and we adopt this value throughout. Note that this formulation differs slightly from Reference [1] in that (7) and (8) are applied throughout the fluid domain. We emphasize that throughout this paper the interpretation of the power of ∇ depends on whether this operator is acting on a scalar or a vector, and in this context the following set of rules should be obeyed (see Reference [6, Chapter 5])

$$\nabla^{2n}\mathbf{u} = \nabla(\nabla^{2n-2}(\nabla \cdot \mathbf{u})), \nabla^{2n+1}\mathbf{u} = \nabla^{2n}(\nabla \cdot \mathbf{u})$$
$$\nabla^{2n}w = \nabla^{2n}w, \qquad \nabla^{2n+1}w = \nabla(\nabla^{2n}w)$$

Inserting (7) and (8) into (5) and neglecting the bottom slope gives the following flat-bottom expression of the kinematic bottom condition, which relates the pseudo-velocity variables $\hat{\mathbf{u}}^*$ and $\hat{w}^*$ to each other

$$\left(1 - \frac{4}{9}\gamma^2\nabla^2 + \frac{1}{63}\gamma^4\nabla^4\right)\hat{w}^* + \left(\gamma\nabla - \frac{1}{9}\gamma^3\nabla^3 + \frac{1}{945}\gamma^5\nabla^5\right)\hat{\mathbf{u}}^* = 0 \tag{10}$$

where $\gamma = (h + \hat{z})$. It is straight-forward to include the variable depth terms (see References [1–3, 7]), however they will not be included in the present work. Combining (10) with (7) applied at $z = \eta$, while also invoking (4) gives a 3×3 system that can be solved for $\hat{\mathbf{u}}^*$ and $\hat{w}^*$ in terms of $\tilde{\mathbf{U}}$ and η. The resulting system of PDEs is given in matrix form as

$$\begin{bmatrix} \mathscr{A}_{11} - \eta_x\mathscr{B}_{11} & \mathscr{A}_2 - \eta_x\mathscr{B}_{12} & \mathscr{B}_{11} + \eta_x\mathscr{A}_1 \\ \mathscr{A}_2 - \eta_y\mathscr{B}_{11} & \mathscr{A}_{22} - \eta_y\mathscr{B}_{12} & \mathscr{B}_{12} + \eta_y\mathscr{A}_1 \\ \mathscr{A}_{01} & \mathscr{A}_{02} & \mathscr{B}_0 \end{bmatrix} \begin{bmatrix} \hat{u}^* \\ \hat{v}^* \\ \hat{w}^* \end{bmatrix} = \begin{bmatrix} \tilde{U} \\ \tilde{V} \\ 0 \end{bmatrix} \tag{11}$$

Here the subscripts x and y denote partial differentiation. The system contains a number of differential operators, which can be found in Appendix A (see also Reference [3]). For now it is sufficient to mention that each operator contains up to either fourth- or fifth-order mixed partial derivatives. This system of operators shall henceforth be referred to as $\mathscr{A}$, and upon discretization this system shall be referred to as $\mathbf{Ax} = \mathbf{b}$. Fuhrman and Bingham [3] have also shown that under the assumption of potential (irrotational) flow such that

$$\frac{\partial u}{\partial y} - \frac{\partial v}{\partial x} = 0 \tag{12}$$

the system simplifies slightly to

$$\mathscr{A} = \begin{bmatrix} \mathscr{A}_1 - \eta_x\mathscr{B}_{11} & -\eta_x\mathscr{B}_{12} & \mathscr{B}_{11} + \eta_x\mathscr{A}_1 \\ -\eta_y\mathscr{B}_{11} & \mathscr{A}_1 - \eta_y\mathscr{B}_{12} & \mathscr{B}_{12} + \eta_y\mathscr{A}_1 \\ \mathscr{A}_{01} & \mathscr{A}_{02} & \mathscr{B}_0 \end{bmatrix} \tag{13}$$

We stress that (12) is a single component of the vorticity vector, and that the other elements (involving z-derivatives) have already been eliminated via the expansion of the velocity

potential in the z-direction in the derivation process. Formulations using $\mathbf{A}$ stemming from (11) and (13) will both be considered in this work.

Having solved for the pseudo-velocities $\hat{\mathbf{u}}^*$ and $\hat{w}^*$ from (11) or (13), $\tilde{w}$ can be computed from (8) applied at $z=\eta$. This can be equivalently expressed in terms of the previously introduced operators as

$$\tilde{w} = \mathscr{A}_1 \hat{w}^* - \mathscr{B}_{11}\hat{u}^* - \mathscr{B}_{12}\hat{v}^* \tag{14}$$

which closes the problem.

3. STABILITY OF THE METHOD OF LINES

A method of lines approach allows for separate consideration of the time integration scheme and the spatial discretization. This has the advantage that stability criterion for any number of time stepping schemes can be obtained simultaneously. The justification is widely known and can be explained by considering a general system of linear differential equations having the form

$$\frac{\partial \mathbf{y}}{\partial t} = \mathbf{J}\mathbf{y} \tag{15}$$

where $\mathbf{y}$ is a vector of time stepping variables, and $\mathbf{J}$ is the linear Jacobian matrix. Substituting the spectral factorization $\mathbf{J}=\mathbf{V}\mathbf{\Lambda}\mathbf{V}^{-1}$ (where $\mathbf{V}$ is a matrix whose columns contain the eigenvectors of $\mathbf{J}$, and $\mathbf{\Lambda}$ is a diagonal matrix of corresponding eigenvalues λ_i) into (15) leads directly to $\partial\mathbf{y}/\partial t = \mathbf{V}\mathbf{\Lambda}\mathbf{V}^{-1}\mathbf{y}$. Multiplying both sides by $\mathbf{V}^{-1}$ and considering that $\mathbf{V}$ is time independent gives $\partial/\partial t(\mathbf{V}^{-1}\mathbf{y}) = \mathbf{\Lambda}(\mathbf{V}^{-1}\mathbf{y})$. Finally, defining a new variable $\mathbf{z}=\mathbf{V}^{-1}\mathbf{y}$, the system becomes $\partial\mathbf{z}/\partial t = \mathbf{\Lambda}\mathbf{z}$ i.e. original system (15) can identically be considered as a number of independent scalar linear ordinary differential equations of the form

$$\frac{\partial z_i}{\partial t} = \lambda_i z_i \tag{16}$$

This diagonalized system can be interpreted as a representation of the original system (15) in the basis of eigenvectors of $\mathbf{J}$ [8]. As a result of this diagonalization the semi-discrete system can be analysed for stability based on the eigenvalues of $\mathbf{J}$ alone.

By considering a single scalar linear test equation of form (16), it can likewise be shown (see e.g. References [8–12]) that for a given time stepping scheme a region of absolute stability can be constructed—often simply called its *stability region*. As a necessary condition for stability, all eigenvalues of $\mathbf{J}$, when amplified by the time step Δt, must lie within the stability region of the respective time stepping scheme. Stability regions for numerous popular time stepping schemes are commonplace, and can be found e.g. in References [9–12]. For brevity they are not re-plotted here.

It is easy to show that a centrally discretized (linear) hyperbolic system will result in a Jacobian matrix having purely imaginary eigenvalues (this is demonstrated for our particular system in Sections 4 and 5). By inspection of various linear stability regions it can immediately be seen that such a scheme will only be conditionally stable under certain time stepping schemes i.e. those whose stability region contains some portion of the imaginary axis. As a demonstration of a conditionally stable scheme which works well in practice we

will consider the classical explicit fourth-order, four stage Runge–Kutta method throughout this paper, though certainly more advanced time stepping methods are available (see e.g. References [13, 14], and the recent comparison in Reference [15]). For completeness, the stability region for this method contains the imaginary interval $(-2.8284\mathrm{i}, 2.8284\mathrm{i})$ and the real interval $(-2.7853, 0)$. For a more complete discussion on the suitability of numerous popular time stepping schemes for systems of this type see Reference [12, p. 209]. We stress that the analysis herein can easily be applied to any number of time integration methods (both explicit and implicit), simply by considering the eigenvalue spectra in the following sections with the stability region of interest.

4. LINEAR FOURIER ANALYSIS

The system of PDEs in the Boussinesq formulation will now be considered in its simplest form i.e. considering linear wave propagation in a single horizontal dimension on a flat bottom. The linearized kinematic and dynamic free surface conditions, respectively, read

$$\frac{\partial \eta}{\partial t} = w_0, \quad \frac{\partial u_0}{\partial t} = -g\frac{\partial \eta}{\partial x} \tag{17}$$

Here u_0 and w_0 are velocities at the still water level $z=0$ in the x- and z-directions, respectively. Similar to Section 2, w_0 is found via a solution of the implicit (flat-bottom) relationship

$$\begin{bmatrix} \mathscr{A}_1 & \mathscr{B}_{11} \\ \mathscr{A}_{01} & \mathscr{B}_0 \end{bmatrix} \begin{bmatrix} \hat{u}^* \\ \hat{w}^* \end{bmatrix} = \begin{bmatrix} u_0 \\ 0 \end{bmatrix} \tag{18}$$

combined with the expression

$$w_0 = \mathscr{A}_1 \hat{w}^* - \mathscr{B}_{11}\hat{u}^* \tag{19}$$

The operators in (18) and (19) are simply one-dimensional representations of those in Appendix A, and contain up to fifth-order partial derivatives in x. Note that in this linearized form, each operator arises from (7) and (8) applied at $z=0$. It can be seen that $\hat{u}^*$ and $\hat{w}^*$ can be eliminated by inserting the solution of (18) directly into (19), which gives an expression for w_0 in terms of u_0

$$w_0 = \frac{(\mathscr{A}_1\mathscr{A}_{01} + \mathscr{B}_0\mathscr{B}_{11})u_0}{\mathscr{A}_{01}\mathscr{B}_{11} - \mathscr{A}_1\mathscr{B}_0} \tag{20}$$

The Fourier (von Neumann) analysis begins by firstly considering each differential operator in discrete form, as stability is purely a property of the discretized equations. In this analysis we consider two centred spatial discretizations. These are the use of second-order finite-difference approximations for each derivative, as well as the use of high-order seven-point approximations for each derivative (order ranging from two to six). Through further substitution of individual Fourier components

$$\eta(j) \Rightarrow \check{\eta}\mathrm{e}^{\mathrm{i}j\theta}, \quad u_0(j) \Rightarrow \check{u}_0\mathrm{e}^{\mathrm{i}j\theta} \tag{21}$$

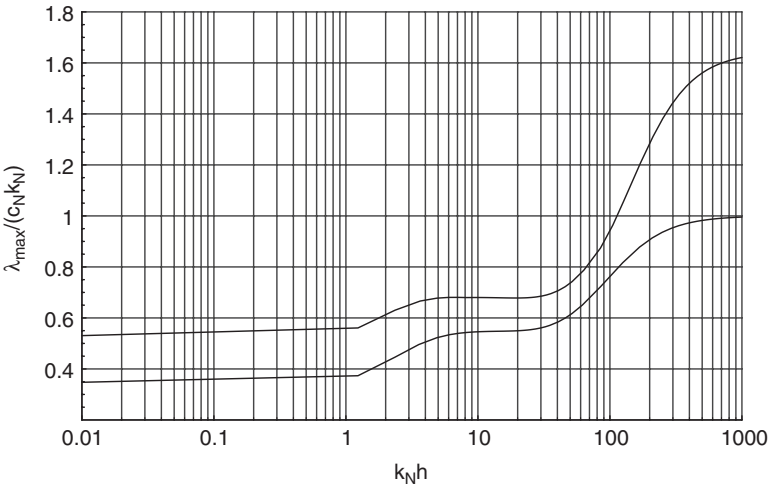

Figure 1. Non-dimensionalized maximum eigenvalues as a function of $k_N h$ from the Fourier analysis in a single horizontal dimension. The top and bottom lines correspond to using high-order (seven-point) and second-order finite difference approximations, respectively.

(where j is the grid point, and $\theta = 2\pi/N$, with N the number of grid points per wavelength) and by inserting (20) into w_0 in (17) the system can be transformed to a semi-discrete form

$$\frac{\partial}{\partial t}\begin{bmatrix} \breve{\eta} \\ \breve{u}_0 \end{bmatrix} = \begin{bmatrix} 0 & \mathscr{J}_{12} \\ \mathscr{J}_{21} & 0 \end{bmatrix}\begin{bmatrix} \breve{\eta} \\ \breve{u}_0 \end{bmatrix} \tag{22}$$

Note that in this form the time stepping variables have changed from η and u_0 to their respective Fourier amplitudes $\breve{\eta}$ and $\breve{u}_0$. It should also be mentioned that the insertion of the Fourier components (21) involves the assumption of periodic boundary conditions. This is often interpreted simply as being applicable to the modelled regions which are sufficiently far from the boundaries such that their effects are minimal [11]. After invoking the Eulerian identity $e^{i\theta} = \cos\theta + i\sin\theta$, it can be shown that $\mathscr{J}_{21} = -ig\sin\theta/\Delta x$ under discretization with second-order finite difference approximations and $\mathscr{J}_{21} = -ig\,(3/2\sin\theta - 3/10\sin(2\theta) + \sin(3\theta)/30)/\Delta x$ under discretization with high-order (seven-point) finite difference approximations. These expressions are simply Fourier space representations of the discrete $-g\partial/\partial x$ operator. Under both discretizations the representation of $\mathscr{J}_{12}$ is extremely long and will not be given here (it is in fact the Fourier space representation of the discretized factor for u_0 in (20)). Given the complexity of this term, the analysis is only practical with a symbolic manipulator (the current analysis has been performed using *Mathematica*™). Note that (22) is precisely of form (15), and thus it is the eigenvalues of this matrix which will govern the linear stability. In the current analysis only integer values for N are considered, which has been found to give reasonable results. As suggested earlier, the eigenvalues are indeed purely imaginary and the maximum computed values are given (non-dimensionalized) in Figure 1 for both discretizations for a wide range of $k_N h$, where $k_N = \pi/\Delta x$ is the Nyquist wave number. The eigenvalues have been non-dimensionalized using the celerity of the Nyquist mode c_N, which

is computed using the embedded linear dispersion relation given in References [1, 2] as

$$c = \sqrt{\frac{g}{k}\left(\frac{sh(k(h+\hat{z}))ch(k\hat{z}) - ch(k(h+\hat{z}))sh(k\hat{z})}{ch(k(h+\hat{z}))ch(k\hat{z}) - sh(k(h+\hat{z}))sh(k\hat{z})}\right)} \tag{23}$$

with

$$ch(\psi) = \left(1 + \frac{4}{9}\psi^2 + \frac{1}{63}\psi^4\right), \quad sh(\psi) = \left(\psi + \frac{1}{9}\psi^3 + \frac{1}{945}\psi^5\right) \tag{24}$$

Note that the y-axis of this figure could identically be replaced with $\lambda_{\max}/\omega_N$, where ω_N is the angular frequency of the Nyquist mode. This plot is given in terms of k_N (rather than e.g. just Δx), to allow for a more direct comparison with the matrix-based analysis (in two horizontal dimensions) in Section 5.

From the Fourier analysis it has been found that the maximum eigenvalue generally occurs with $\theta = \pi/2$ (i.e. a mode having four grid points per wavelength, or twice the Nyquist wavelength, thus $k_{\text{critical}} = k_N/2$). This has been found to be generally true under discretization with second-order finite difference approximations, and true for $k_N h < 100$ with high-order finite difference approximations. For $k_N h > 100$ under the high-order discretization the critical mode shifts to $\theta = 2\pi/3$ i.e. one having three grid points per wavelength. The highest frequency (Nyquist) mode actually results in a zero eigenvalue, and is thus *always* linearly stable under these discretizations (this can readily be seen e.g. by inserting $\theta = \pi$ into the previously given expressions for $\mathscr{J}_{21}$). In general it is seen that the high-order spatial discretization results in larger eigenvalues, and will consequently have more restrictive stability properties. These differences are more dramatic in very shallow water, and become less pronounced (percentage-wise) as $k_N h$ increases, at least up to $k_N h \approx 100$. We stress that as shown in Reference [3], this does not necessarily result in greater overall efficiency, as the use of the higher-order finite difference approximations can allow for significant reductions in the number of grid points required for a desired accuracy.

Upon closer examination of Figure 1 some distinct regions can be observed. With $k_N h < 1$ it is seen that the non-dimensionalized eigenvalue flattens, corresponding to the point where the most critical mode becomes non-dispersive. Within the range $1 < k_N h < 2\pi$ a transition region is apparent, as the critical mode gradually moves from shallow water to the practical deep-water limit. In the range $2\pi < k_N h < 40$ the curves again level, as the celerity of the critical mode becomes insensitive to changes in the depth. Finally, at $k_N h > 40$ the curves again begin to rise, corresponding roughly to the point where the linear dispersive properties of the critical mode begin to fail with respect to linear wave theory (c_N becomes significantly underestimated). Note that in most practical applications $k_N h > \pi$ i.e. at least the highest resolved frequency mode is beyond the practical deep-water limit. Practical applications in intermediate to very deep water are typically in the range $10 < k_N h < 500$.

The maximum time step $\Delta t_{\max}$ that can be taken due to stability constraints is found as follows: Given a spatial discretization, k_N can readily be computed, as can c_N from (23). With k_N and c_N known, the maximum eigenvalue $\lambda_{\max}$ can be obtained from Figure 1. The (hyperbolic) Courant number is then

$$r_h = \lambda_{\max} \Delta t \tag{25}$$

Thus, the maximum Courant number $r_{h,\max}$ allowable for stability is simply the point where the stability region of the time stepping scheme of interest crosses the imaginary axis (note that certain implicit schemes will therefore be linearly unconditionally stable). Hence, $\Delta t_{\max}$ can easily be computed from (25) i.e. $\Delta t_{\max} = r_{h,\max}/\lambda_{\max}$. From this section linear stability criterion can be established for both finite difference discretizations considered in combination with any number of time stepping methods.

5. LINEAR MATRIX-BASED ANALYSIS

As an alternative to the Fourier techniques used in Section 4 an entirely numerical, matrix-based approach can be adopted—the actual Jacobian matrix **J** can be constructed and its eigenvalues computed directly. This approach has the advantage of being very general e.g. any effects from boundary conditions are inherently included in the analysis. It is even fairly straight-forward to extend the analysis to include the effects of the non-linear terms (at least locally), which is the ultimate motivation here. Note that for the remainder of this paper combined Dirichlet and Neumann boundary conditions are used to create closed boundaries on a rectangular domain, as in Reference [3]. Specifically, this corresponds to imposing $u = 0$, $\partial v/\partial x = 0$, $\partial w/\partial x = 0$, and $\partial \eta/\partial x = 0$ along x-boundaries; and $\partial u/\partial y = 0, v = 0$, $\partial w/\partial y = 0$, and $\partial \eta/\partial y = 0$ along y-boundaries. These conditions are imposed simply by reflecting the finite difference coefficients evenly for Neumann boundary conditions and oddly for Dirichlet boundary conditions. Although the approach in this section is completely numerical, for convenience the differential operators are given in continuous form in much of what follows.

To begin the linearized flat-bottom system in two horizontal dimensions will be considered. The free surface conditions now consist of (17) combined with

$$\frac{\partial v_0}{\partial t} = -g\frac{\partial \eta}{\partial y} \tag{26}$$

To form the Jacobian matrix **J** it is necessary to express the linearized free surface equations explicitly in terms of the time stepping variables η, u_0, and v_0. With this system, however, w_0 is normally found via an implicit relationship i.e. a solution of the system $\mathbf{Ax} = \mathbf{b}$, where $\mathbf{x}^{\mathrm{T}} = [\hat{\mathbf{u}}^*, \hat{\mathbf{v}}^*, \hat{\mathbf{w}}^*]$ and $\mathbf{b}^{\mathrm{T}} = [\mathbf{u}_0, \mathbf{v}_0, \mathbf{0}]$, combined with

$$w_0 = \mathscr{A}_1 \hat{w}^* - \mathscr{B}_{11}\hat{u}^* - \mathscr{B}_{12}\hat{v}^* \tag{27}$$

which is simply the linearized form of (14). This can easily be converted into an explicit expression, however, simply by taking $\mathbf{Z} = \mathbf{A}^{-1}$, which leads obviously to $\mathbf{x} = \mathbf{Zb}$. Note that here **Z** is a dense matrix. Considering **Z** in block form, this operation can be written as

$$\begin{bmatrix} \hat{u}^* \\ \hat{v}^* \\ \hat{w}^* \end{bmatrix} = \begin{bmatrix} \mathscr{Z}_{11} & \mathscr{Z}_{12} & \mathscr{Z}_{13} \\ \mathscr{Z}_{21} & \mathscr{Z}_{22} & \mathscr{Z}_{23} \\ \mathscr{Z}_{31} & \mathscr{Z}_{32} & \mathscr{Z}_{33} \end{bmatrix} \begin{bmatrix} u_0 \\ v_0 \\ 0 \end{bmatrix} \tag{28}$$

Inserting (28) into (27) gives the following explicit expression for the determination of w_0 from u_0 and v_0

$$w_0 = \mathscr{A}_1\mathscr{Z}_{31}u_0 + \mathscr{A}_1\mathscr{Z}_{32}v_0 - \mathscr{B}_{11}\mathscr{Z}_{11}u_0 - \mathscr{B}_{11}\mathscr{Z}_{12}v_0 - \mathscr{B}_{12}\mathscr{Z}_{21}u_0 - \mathscr{B}_{12}\mathscr{Z}_{22}v_0 \tag{29}$$

Thus, the linearized system can now indeed be written in a semi-discrete form as

$$\frac{\partial}{\partial t}\begin{bmatrix}\eta\\ u_0\\ v_0\end{bmatrix} = \begin{bmatrix}0 & \frac{\partial}{\partial u_0}\left(\frac{\partial \eta}{\partial t}\right) & \frac{\partial}{\partial v_0}\left(\frac{\partial \eta}{\partial t}\right)\\ -g\frac{\partial}{\partial x} & 0 & 0\\ -g\frac{\partial}{\partial y} & 0 & 0\end{bmatrix}\begin{bmatrix}\eta\\ u_0\\ v_0\end{bmatrix} \tag{30}$$

where substituting (29) into w_0 from (17) leads to

$$\frac{\partial}{\partial u_0}\left(\frac{\partial \eta}{\partial t}\right) = \mathscr{A}_1\mathscr{Z}_{31} - \mathscr{B}_{11}\mathscr{Z}_{11} - \mathscr{B}_{12}\mathscr{Z}_{21} \tag{31}$$

$$\frac{\partial}{\partial v_0}\left(\frac{\partial \eta}{\partial t}\right) = \mathscr{A}_1\mathscr{Z}_{32} - \mathscr{B}_{11}\mathscr{Z}_{12} - \mathscr{B}_{12}\mathscr{Z}_{22} \tag{32}$$

Note that the 3×3 system in (30) (when discretized) is the Jacobian matrix **J** for this system, and in this linearized form is time constant.

5.1. Comparison of rotational and irrotational formulations

As shown in Section 2 (see also Reference [3]), this Boussinesq method can be written in either rotational or irrotational form in two horizontal dimensions, and both will be considered here. The analyses are quite similar, however, with the only difference being in the form of the matrix **A**. Figure 2 plots computed maximum (non-dimensionalized) eigenvalues (computed using the MATLAB® `eig` function) for both the rotational and irrotational formulations under all four finite difference discretizations considered with the Boussinesq model in Reference [3]. These include the use of all second-order finite difference approximations, as well as stencils containing 25, 37, and 49 points, where each approximation is allowed to have the maximum formal accuracy possible on each stencil. All computations use a 21×21 computational grid (giving a Jacobian matrix of dimension $21\times 21\times 3 = 1323$), which has been found in practice to be sufficiently large for the purposes of this analysis. This grid provides three full stencil widths in both horizontal directions, and comparisons with systems arising from larger grids have been found to result in essentially the same spread of eigenvalues. In two horizontal dimensions k_N is the modulus of the Nyquist wave number vector $\mathbf{k}_N = \langle \pi/\Delta x, \pi/\Delta y\rangle$, defined as

$$k_N = \sqrt{\left(\frac{\pi}{\Delta x}\right)^2 + \left(\frac{\pi}{\Delta y}\right)^2} \tag{33}$$

Note that this two-dimensional modulus will tend to be larger than in a single dimension for a given spatial discretization (for example, with $\Delta x = \Delta y$ the two-dimensional k_N will always be larger than that from a single horizontal dimension with equivalent Δx by a factor $\sqrt{2}$). Again the high-order finite difference approximations are somewhat more restrictive

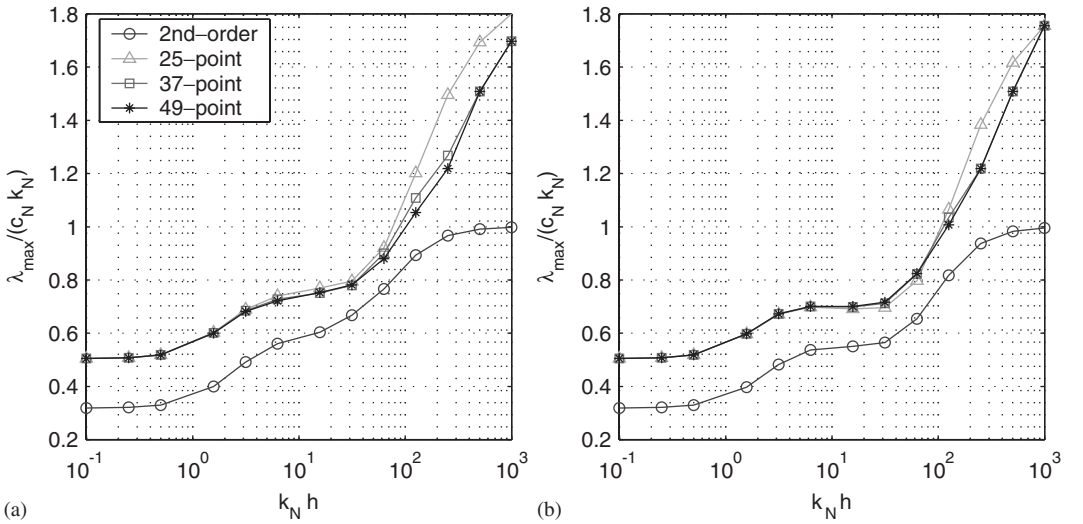

Figure 2. Non-dimensionalized maximum eigenvalues for the linear system (in two horizontal dimensions) as a function of $k_N h$ for (a) the rotational formulation and (b) the irrotational formulation.

(i.e. result in larger eigenvalues) than are second-order finite difference approximations. The differences between the other finite difference stencils, as well as in the two formulations are relatively minor, with slight differences becoming apparent at higher values of $k_N h$. The resulting figures (especially for the irrotational formulation) are remarkably similar to Figure 1, as the two-dimensionality and the closed boundary conditions seem to play a relatively minor role as far as the overall numerical stability is concerned. Values for the eigenvalues (and thus for the determination of r_h) will be taken directly from Figure 2 for the remainder of this work.

As examples from the linearized system Plate 1 shows the eigenvalue distributions for three different values of r_h arising from a rotational system using the 37-point finite difference stencil with $k_N h = 20\pi$. From these plots it can once again be seen that the eigenvalues are indeed purely imaginary, as discussed previously in Section 4. For demonstration purposes, the stability region from the explicit fourth-order Runge–Kutta time stepping scheme is shown (likewise on all remaining figures), and the maximum (and minimum) eigenvalues can be seen to lie on the curve at the limiting $r_h = 2.8284$. This stability limit is also confirmed using the numerical model in Section 8.1.

6. LOCAL NON-LINEAR MATRIX-BASED ANALYSIS

While numerical experiments confirm the previous findings for the linearized system, experience with the non-linear model has shown that in the absence of numerical dissipation, simulations are generally *unstable*. Thus the linear analyses, perhaps unsurprisingly, do not give a complete account of the non-linear behaviour. In other words, the linear constraints are no doubt *necessary*, but by no means are they *sufficient* for the general stability of

non-linear simulations. In an attempt to gain insight into this behaviour, the matrix-based stability analysis from Section 5 is extended to include the non-linear terms in this section.

Consider the non-linear formulation outlined in Section 2. Recall also that diffusive terms with diffusion coefficient D have been added to each of the free surface equations (1)–(3). This serves as a convenient means of adding numerical dissipation to the system, the effect of which will be demonstrated in Section 6.3. These diffusive terms also necessitate an additional stability criterion based on the parabolic Courant number, defined here as

$$r_p = \delta D k_{\mathrm{N}}^2 \Delta t \tag{34}$$

This definition for r_p is convenient, as it corresponds precisely to the (negative) real spread of the linear eigenvalue spectrum. Calculations with the linearized system have shown that reasonable values for the coefficient δ are 0.4053 and 0.6124 when using second-order and higher-order finite difference approximations, respectively. Note that when $r_p = 0$ the system is free of any added dissipation.

For non-linear analysis purposes it is common to investigate the eigenvalues of the Jacobian matrix using temporally local coefficients. Hence, we inherently assume that the local behaviour of the system is modelled well by the variational equation $\partial \mathbf{y}/\partial t = \partial \mathbf{y}_n/\partial t + \mathbf{J}_n(\mathbf{y} - \mathbf{y}_n)$, where n is the local time level. The 3×3 Jacobian matrix $\mathbf{J}$ is now generally defined as

$$\mathbf{J} = \begin{bmatrix} \frac{\partial}{\partial \eta}\left(\frac{\partial \eta}{\partial t}\right) & \frac{\partial}{\partial \tilde{U}}\left(\frac{\partial \eta}{\partial t}\right) & \frac{\partial}{\partial \tilde{V}}\left(\frac{\partial \eta}{\partial t}\right) \\ \frac{\partial}{\partial \eta}\left(\frac{\partial \tilde{U}}{\partial t}\right) & \frac{\partial}{\partial \tilde{U}}\left(\frac{\partial \tilde{U}}{\partial t}\right) & \frac{\partial}{\partial \tilde{V}}\left(\frac{\partial \tilde{U}}{\partial t}\right) \\ \frac{\partial}{\partial \eta}\left(\frac{\partial \tilde{V}}{\partial t}\right) & \frac{\partial}{\partial \tilde{U}}\left(\frac{\partial \tilde{V}}{\partial t}\right) & \frac{\partial}{\partial \tilde{V}}\left(\frac{\partial \tilde{V}}{\partial t}\right) \end{bmatrix} \tag{35}$$

The determination of the individual components of this matrix is rather complicated, and is addressed in Appendix B. It should be stressed that such an extension of linear theory to a non-linear setting is far from an exact practice, and due care should be taken in the interpretation of the results. Adding to the complication, it is impossible to examine every possible physical situation. Despite these drawbacks, it is often possible to demonstrate qualitative tendencies using such a local analysis, and this is the aim here.

All results in this section use linear standing wave initial conditions on a flat bottom with waveheight H and wavelength (in both x- and y-directions) $L = 1$ m. This gives a linear deep-water period $T = 0.6730$ s. Each simulation uses $\Delta x = \Delta y = L/20 = 0.05$ m, and $\Delta t = T/20 = 0.03365$ s, and the results shown are from the 22nd time step (frozen in time), which has been chosen arbitrarily to provide conditions roughly in mid-cycle. Computations are again on a 21×21 grid, and use the 37-point finite difference stencil. Results using the other stencils, as well as at other time levels have been found to be qualitatively similar. All results in this section will be given in terms of the dimensionless quantities kh (the relative depth of the primary wave), either H/h or H/L (the shallow- or deep-water non-linearity, respectively), and $k_{\mathrm{N}}h$ (the spatial discretization). As reference values, the practical deep water limit is conventionally $kh = \pi$, and upper limits for the respective non-linearities (before wave breaking) are $H/h \approx 0.8$ and $H/L \approx 0.14$ in shallow and deep water. Experience has shown that the rotational and irrotational formulations behave somewhat differently in cases having significant non-linearity, particularly in deep water where the irrotational formulation

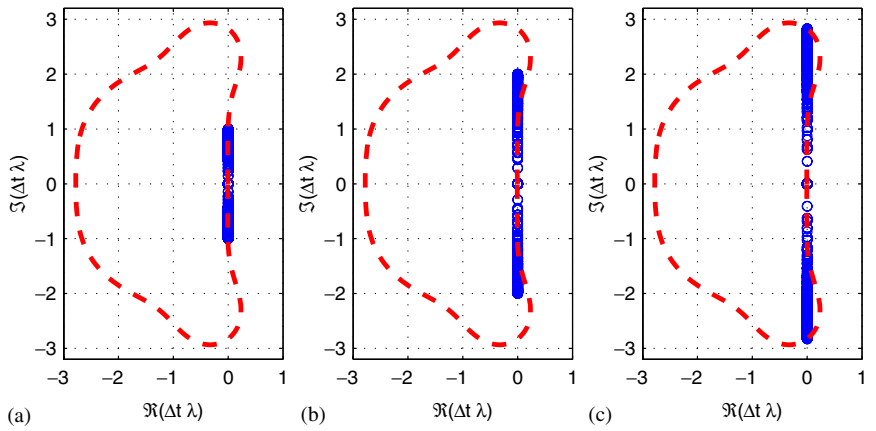

Plate 1. Eigenvalues of $\Delta t\mathbf{J}$ for the linear rotational formulation with $k_{\mathrm{N}}h = 20\pi$ and (a) $r_h = 1$, (b) $r_h = 2$, and (c) $r_h = 2.8284$.

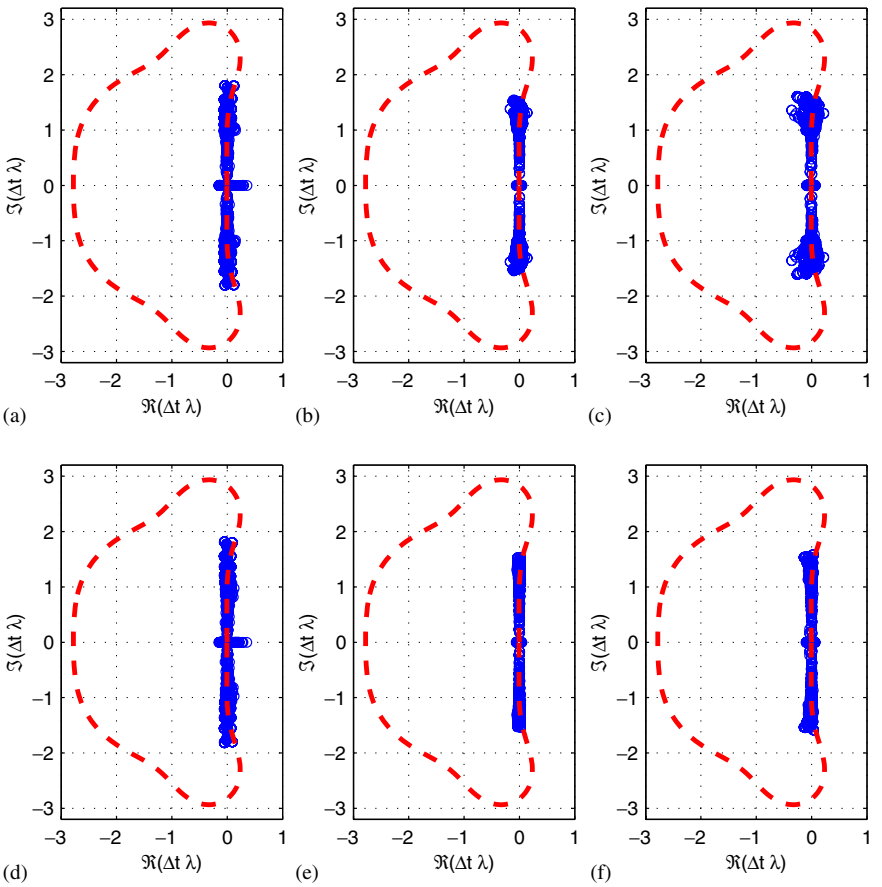

Plate 2. Eigenvalues of $\Delta t\mathbf{J}$ with $r_h = 1.5$ for the rotational (top) and irrotational (bottom) formulations with (a), (d) $kh = \pi/5$, $H/h = 0.7071$, $k_{\mathrm{N}}h = 2\pi$; (b), (e) $kh = 2\pi$, $H/L = 0.05$, $k_{\mathrm{N}}h = 20\pi$; and (c), (f) $kh = 2\pi$, $H/L = 0.10$, $k_{\mathrm{N}}h = 20\pi$.

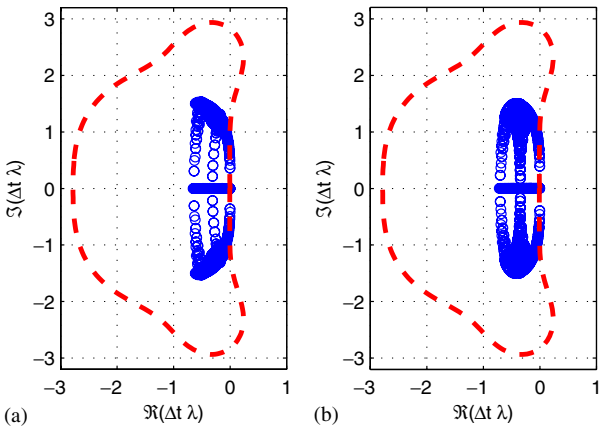

Plate 3. Eigenvalues of $\Delta t\mathbf{J}$ with $kh = 2\pi$, $H/L = 0.05$, $k_N h = 20\pi$, $r_h = 1.5$, and $D = 0.002\,\mathrm{m/s^2}$ for (a) the rotational ($r_p = 0.6338$) and (b) the irrotational formulation ($r_p = 0.6934$).

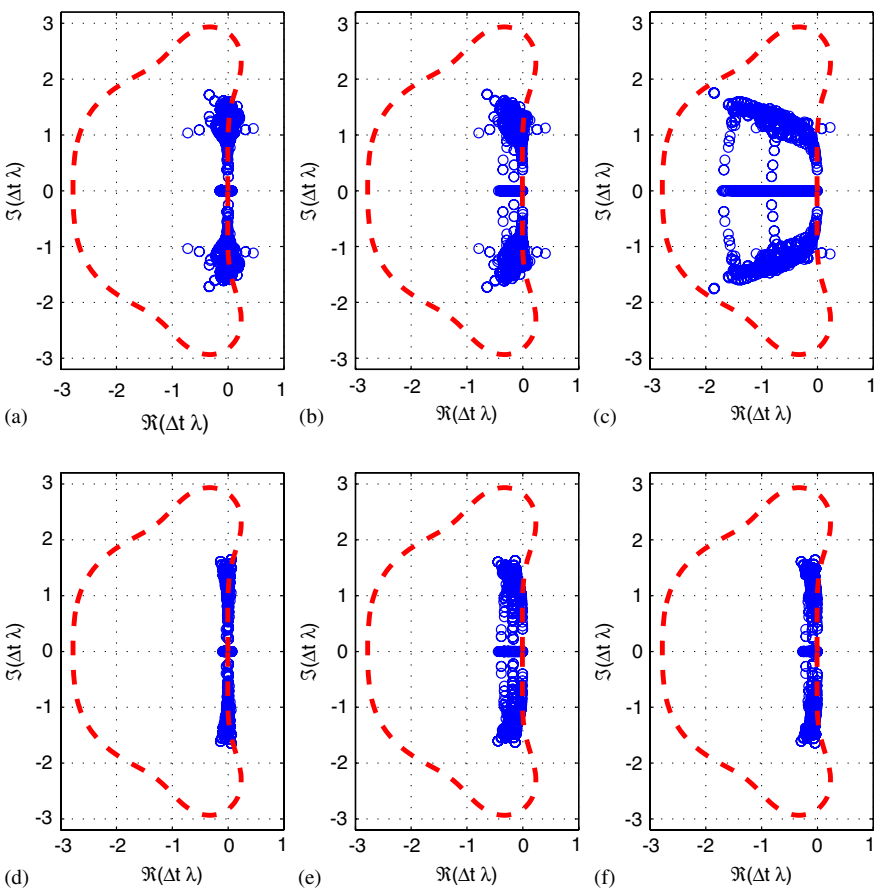

Plate 4. Eigenvalues of $\Delta t\mathbf{J}$ for the rotational (top) and irrotational (bottom) formulations with $kh = 4\pi$, $H/L = 0.12$, $k_N h = 40\pi$, $r_h = 1.5$, and (a), (d) $D = 0\,\mathrm{m^2/s}$; (b), (e) $D = 0.001\,\mathrm{m^2/s}$ ($r_p = 0.3327$, 0.3561); (c) $D = 0.005\,\mathrm{m^2/s}$ ($r_p = 1.6636$); and (f) $D = 5 \times 10^{-4}\,\mathrm{m^2/s}$ ($r_p = 0.1780$).

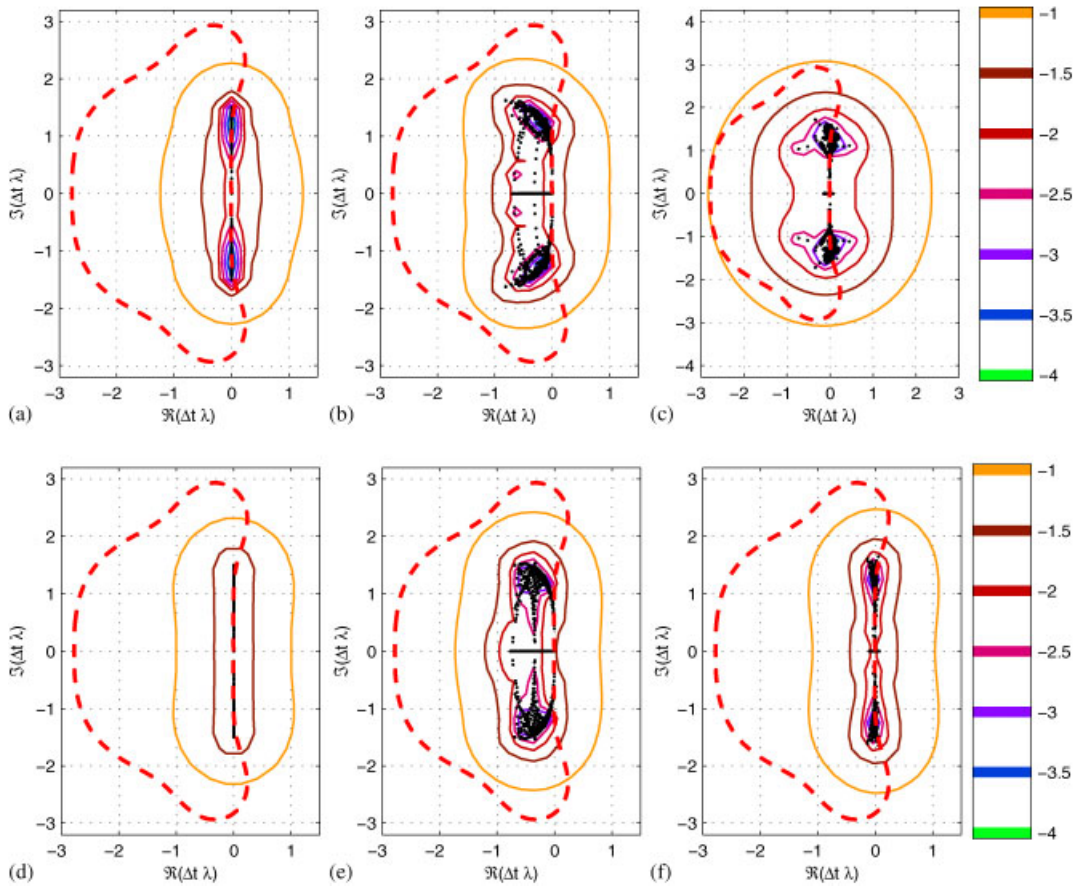

Plate 5. Pseudospectra ($r_h = 1.5$) of $\Delta t\mathbf{J}$ for the (top) rotational and (bottom) irrotational formulations for (a), (d) linear matrices with $k_N h = 4\pi$; (b), (e) non-linear matrices with $kh = 2\pi$, $H/L = 0.10$, $k_N h = 20\pi$, $D = 0.002$ m^2/s ($r_p = 0.6338, 0.6934$); and (c), (f) non-linear matrices with $kh = 4\pi$, $H/L = 0.12$, $k_N h = 40\pi$, $D = 0$ m^2/s. The values for the colorbars correspond to the base-10 power of ε i.e. $\varepsilon = 10^{-4}, \ldots, 10^{-1}$.

has been found to be much more stable. Both systems will therefore be analysed independently in what follows.

6.1. The presence of non-linear instabilities

Plate 2 shows eigenvalue distributions from both the rotational and irrotational formulations under a variety of physical situations (i.e. varying depth and non-linearity) with $r_h = 1.5$ and $r_p = 0$ (i.e. no added dissipation). Here it is clearly seen that the addition of the non-linear terms has produced scattered eigenvalues protruding into the right half of the complex plane, indicating the presence of local exponentially growing modes. This suggests that under these discretizations the system may indeed be susceptible to non-linear instabilities, which is in fact the case in practice. This analysis indicates that in both formulations the strength of the instabilities increases with non-linearity, with the rotational system exhibiting faster growth of the locally unstable modes (i.e. eigenvalues farther away from the linear stability region) in deep water. Note also that the imaginary spread of eigenvalues is somewhat greater than would be expected from the linear analysis, and that this trend is amplified as the non-linearity is increased. This is particularly apparent in Plate 2, parts (a), (c) and (d), (f), which have the strongest non-linearity (recall that the hyperbolic Courant number r_h refers to the expected imaginary spread of eigenvalues from the linear analysis). This trend is consistent with the amplitude dispersion characteristics of non-linear waves—non-linear waves travel faster than linear waves having the same wavelength and water depth.

6.2. The effect of numerical dissipation

The eigenvalue distributions shown in Plate 2 for the non-linear model indicate that simulations are locally unstable. In practice, however, we find that the addition of minor levels of numerical dissipation will generally stabilize the non-linear simulations. The effect of such dissipation on the eigenvalue spectra is demonstrated in Plate 3, where now the diffusion coefficient has been increased to $D = 0.002\ \mathrm{m}^2/\mathrm{s}$. These plots can be compared with Plate 2, parts (b) and (e) with $D = 0\ \mathrm{m}^2/\mathrm{s}$. Clearly (as should be expected) the diffusive terms tend to move the eigenvalue distributions to the left half of the complex plane, stabilizing the schemes (at least locally). The chosen value for D in Plate 3 is roughly the necessary value to locally stabilize each of the distributions.

The use of similar *dissipative interfaces* is commonplace in the numerical modelling community, and is discussed e.g. in References [11, 16]. In general it is felt that the effects shown in Plate 3 on the eigenvalue distributions are qualitatively representative for any number of dissipative interfaces. Other methods for introducing numerical dissipation include Fischer-type semi-discretization [17], which has been considered in the numerical analysis of an alternative form of Boussinesq equations in Reference [18], as well as the application of Savitzky–Golay smoothing filters [19, 20], which have been used successfully in the current model e.g. in References [1, 3, 21].

6.3. Comparison of rotational and irrotational formulations

As noted previously, rotational simulations having high deep-water non-linearity have been found in practice to be much more difficult to stabilize than those using the irrotational formulation. This is especially true on refined grids i.e. where $k_N h$ is relatively large. In an attempt

to provide insight into this observation Plate 4 shows eigenvalue distributions for both formulations with $kh = 4\pi$, $k_N h = 40\pi$, and $H/L = 0.12$. Clearly, both simulations appear locally unstable in the absence of any numerical dissipation, as seen in Plate 4, parts (a) and (d), though this is much less pronounced for the irrotational system (Plate 4(d)). Plates 4(b)–(c) and (e)–(f) give quite dramatic evidence that the rotational system is much more difficult to stabilize in these highly non-linear, deep-water situations. Indeed, as shown in Plates 4(b)–(c), the rotational formulation still retains some locally unstable eigenvalues at relatively high levels of dissipation i.e. up to $D = 0.005\,\mathrm{m}^2/\mathrm{s}$. Closer (visual) inspection of the associated eigenvectors has revealed that these modes seemingly contain somewhat lower frequencies, and thus are not as easily damped by the diffusive terms. The irrotational formulation, on the other hand, is locally stabilized under much lower values of D, as shown in Plates 4(e)–(f). This analysis provides a possible explanation for these difficulties with the rotational formulation, and shows at least locally that the irrotational formulation is much more receptive to dissipation. Based on this analysis (as well as experience) the irrotational formulation is seemingly preferable in simulations having high deep-water non-linearity, so long as the formulation is applicable. Remarkably, Plate 4(f), with $H/L = 0.12$ and $kh = 4\pi$ shows that the necessary value for the diffusion coefficient in this example is roughly $D = 5 \times 10^{-4}\,\mathrm{m}^2/\mathrm{s}$—significantly less than the necessary value of $0.002\ \mathrm{m}^2/\mathrm{s}$ in Plate 3(b) with $H/L = 0.05$ and $kh = 2\pi$. This suggests that the non-linear stability properties of the irrotational formulation actually improve with increasing $k_N h$!

7. ANALYSIS OF PSEUDOSPECTRA

In recent years the concept of the *pseudospectra* of a matrix has arisen as a tool to help understand the behaviour of non-normal matrices (i.e. matrices whose eigenvectors do not form an orthogonal basis). This is important, as cases having severe non-normality can result in behaviour that is not always consistent with what is predicted by an analysis of eigenvalues alone. If λ is an eigenvalue of $\mathbf{J}$, then $\|(\lambda\mathbf{I} - \mathbf{J})^{-1}\|$ is conventionally regarded to be infinite. This begs the question: What if $\|(\lambda_\varepsilon\mathbf{I} - \mathbf{J})^{-1}\|$, $\lambda_\varepsilon \neq \lambda$ is finite, but very large? This pattern of thinking leads to the following definition for the pseudospectra of a matrix [22]:

$$\Lambda_\varepsilon(\mathbf{J}) = \{\lambda_\varepsilon \in \mathbb{C} : \|(\lambda_\varepsilon\mathbf{I} - \mathbf{J})^{-1}\| \geqslant \varepsilon^{-1}\} \tag{36}$$

The pseudospectra of a matrix are thus useful in describing the sensitivity of the eigenvalues to minor perturbations in the original matrix. If a matrix is normal then its two-norm ε-pseudospectrum consists of closed balls of radius ε surrounding the eigenvalues [23]. As the non-normality increases, however, the pseudospectra may deviate far more significantly from the eigenvalues, sometimes by many orders of magnitudes. Pseudospectra have provided valuable insight into numerous issues e.g. that of hydrodynamic stability [24–27]. Issues concerning their computation can be found e.g. in References [28, 29]. For more detailed discussions of pseudospectra as well as numerous examples see References [8, 22, 23, 29].

This issue is explored for the current system using the EigTool package for MATLAB®. A detailed description of this package can be found in References [28, 29]. Pseudospectra from a number of matrices for both rotational and irrotational formulations are shown in Plate 5. From these plots it can be seen that these matrices are only moderately non-normal, which is itself comforting and useful information. This can be seen e.g. by considering that the contours

corresponding to $\varepsilon = 10^{-1}$ deviate from the original spread of eigenvalues typically by a length of $10^0 = 1$, or roughly 10 times what would be expected for a normal matrix. Pseudospectra from the linear models in quite deep water (Plates 5(a) and 5(d) with $k_N h = 40\pi$) show that the eigenvalues from the rotational system are slightly more sensitive to perturbations than from the irrotational formulation, deviating noticeably from the eigenvalues at much lower values of ε. Interestingly, the problematic area in the (non-linear) rotational spectrum seems to already be properly identified in the linearized pseudospectrum in Plate 5(a). In practice we do not observe deviations from the eigenvalue analysis with either system, suggesting that the eigenvalues reasonably characterize the discrete systems at this moderate level of non-normality. Plates 5(b) and (e) show pseudospectra arising from locally stabilized matrices in moderately deep water ($kh = 2\pi$, $k_N h = 20\pi$) with high non-linearity ($H/L = 0.10$). The differences between the two formulations are again not too severe, with the rotational formulation having a slightly larger spread. Notably, while the eigenvalues from Plates 5(a)–(b) and (d)–(e) lie within the stability region, the pseudospectra protrude to the right half of the complex plane, at least for the larger values of ε. However, as the non-normality of the systems in Plates 5(b) and (e) is roughly equivalent to that from Plates 5(a) and (d), we do not expect significant deviations from the eigenvalue analysis with these discretizations. More dramatic differences become apparent when $k_N h$ is increased, as can be seen in a comparison of Plates 5(c) and (f), with $k_N h = 40\pi$, $kh = 4\pi$, $H/L = 0.12$. As Plate 5(f) demonstrates, the irrotational formulation exhibits virtually no dependence on increasing $k_N h$, whereas the rotational system (Plate 5(c)) demonstrates a significant increase in its non-normality (the real pseudospectral radius roughly doubles). This suggests that the non-normality of the rotational formulation may play an increasing role in de-stabilizing highly non-linear deep-water simulations as the grid is refined. However, as shown in Section 6.3 (Plate 4), the eigenvalues already suggest stability problems in these instances.

8. NUMERICAL EXPERIMENTS

The previous findings from both the linear and non-linear analyses will now be tested in a series of numerical experiments. All experiments in this section use linear standing wave initial conditions, and results are again presented in terms of the previously introduced dimensionless quantities. The experiments use a 21×21 grid, and consider a single wavelength $L = 1$ m in both x- and y-directions, with $\Delta x = \Delta y = L/20 = 0.05$ m. All simulations use the 37-point finite difference stencil combined with the explicit fourth-order, four-stage Runge–Kutta time stepping scheme. Results from Figure 2 are again used for the determination of the hyperbolic Courant number r_h.

8.1. Linear experiments

Table I provides a summary of a series of experiments with the linear model for both rotational and irrotational formulations. Simulations are deemed 'stable' after running 10 000 time steps with no sign of instabilities. Recall that the necessary stability limits for this scheme are $r_h < 2.8284$ (corresponding to the imaginary limit) and $r_p < 2.7853$ (corresponding the negative real limit), assuming the eigenvalues span either the imaginary or (negative) real axes separately. This is controlled in these experiments through the choice of time step Δt and

Table I. Summary of numerical experiments with the linear model.

				Rotational			Irrotational		
$k_N h$	r_h	r_p	S/U	Δt (s)	D (m^2/s)	n_u	Δt (s)	D (m^2/s)	n_u
2π	2.8	0	S	0.1304	0	—	0.1355	0	—
2π	2.9	0	U	0.1350	0	448	0.1403	0	456
20π	2.8	0	S	0.1223	0	—	0.1338	0	—
20π	2.9	0	U	0.1267	0	435	0.1386	0	430
40π	2.8	0	S	0.1284	0	—	0.1375	0	—
40π	2.9	0	U	0.1330	0	421	0.1424	0	420
20π	0.1	2.7	S	0.004369	0.1278	—	0.004780	0.1168	—
20π	0.1	2.9	U	0.004369	0.1373	461	0.004780	0.1255	461

Note: The column heading S/U refers to the simulation being either stable/unstable. The variable n_u refers to the time step where the simulations go unstable (taken here as when a NaN is detected).

diffusion coefficient D i.e. when r_h is varied $r_p = 0$, and when r_p is varied r_h is kept small. Here it can clearly be seen that the numerical results match extremely well with the linear stability criterion outlined previously in Sections 4 and 5 for both hyperbolic and parabolic courant numbers. Simulations with the same unstable Courant numbers for both formulations can in fact be seen to go unstable at approximately the same time. These models behave as predicted by the analysis, and the results are not discussed further.

8.2. Non-linear experiments

Tables II and III provide results from a series of non-linear simulations, where the depth and non-linearity are varied for both rotational and irrotational formulations, respectively. These simulations use an unrestarted GMRES [30] algorithm for solutions of $\mathbf{Ax} = \mathbf{b}$ (preconditioned with the linearized matrix, as presented in Reference [3]), with a relative residual error tolerance $r = \|\mathbf{b} - \mathbf{Ax}\|_2 / \|\mathbf{b}\|_2$ of 10^{-6}. Simulations are deemed 'stable' after progressing 5000 time steps with no noticeable evidence of instabilities. For all of the non-linear experiments $r_h = 1.0$ is used to prevent numerical dissipation from the time stepping scheme (at approximately this level lobes from the stability region extend to the right half of the complex plane, effectively resulting in a dissipative scheme).

From these experiments it can be seen that the results match qualitatively with the local non-linear analysis of Section 6. As predicted in Section 6.1, although linearly stable, the simulations generally suffer from non-linear instabilities in the absence of numerical dissipation. Consistent with Section 6.2 (see Plate 3), simulations with either formulation require roughly the same level of dissipation for stabilization in cases with moderate deep-water non-linearity (consider the cases with $kh = 2\pi$, $H/L = 0.05$). Consistent with Section 6.3, it is also shown that the irrotational formulation is much easier to stabilize than is the rotational formulation when the deep-water non-linearity is high, particularly with large $k_N h$. For example, the irrotational simulations with $k_N h = 40\pi$, $kh = 4\pi$ surprisingly require no added dissipation to maintain stability, while similar rotational simulations quickly go unstable. The numerical experiments also indicate that the rotational formulation is somewhat easier to stabilize in shallow water (consider the results with $kh = \pi/5$). Note that these shallow-water simulations are actually very non-linear, with $H/h = 0.7071$. This difference is not as severe as in deep

Table II. Summary of numerical experiments with the non-linear rotational model.

$k_N h$	kh	H/L	Δt (s)	D (m^2/s)	r_p	S/U	n_u
2π	$\pi/5$	0.05	0.04655	0	0	U	2310
2π	$\pi/5$	0.05	0.04655	10^{-6}	2.25×10^{-4}	U	2440
2π	$\pi/5$	0.05	0.04655	10^{-5}	2.25×10^{-3}	S	—
20π	2π	0.05	0.04369	0	0	U	2960
20π	2π	0.05	0.04369	10^{-5}	2.11×10^{-3}	U	3620
20π	2π	0.05	0.04369	10^{-4}	2.11×10^{-2}	S	—
20π	2π	0.10	0.04369	0	0	U	510
20π	2π	0.10	0.04369	10^{-4}	2.11×10^{-2}	U	980
20π	2π	0.10	0.04369	10^{-3}	2.11×10^{-1}	S	—
20π	2π	0.12	0.04369	0	0	U	360
20π	2π	0.12	0.04369	10^{-4}	2.11×10^{-2}	U	560
20π	2π	0.12	0.04369	10^{-3}	2.11×10^{-1}	S	—
40π	4π	0.12	0.04587	0	0	U	230
40π	4π	0.12	0.04587	10^{-4}	2.22×10^{-2}	U	570
40π	4π	0.12	0.04587	10^{-3}	2.22×10^{-1}	S	—

Note: All simulations use $r_h = 1.0$. The column headings are the same as used in Table I. Here the variable n_u refers to first time step where a solution of $\mathbf{Ax} = \mathbf{b}$ exceeds 200 iterations.

Table III. Summary of numerical experiments with the non-linear irrotational model.

$k_N h$	kh	H/L	Δt (s)	D (m^2)/s	r_p	S/U	n_u
2π	$\pi/5$	0.05	0.04838	0	0	U	1030
2π	$\pi/5$	0.05	0.04838	10^{-5}	2.34×10^{-3}	U	1180
2π	$\pi/5$	0.05	0.04838	10^{-4}	2.34×10^{-2}	S	—
20π	2π	0.05	0.04780	0	0	U	2270
20π	2π	0.05	0.04780	10^{-5}	2.31×10^{-3}	U	2520
20π	2π	0.05	0.04780	10^{-4}	2.31×10^{-2}	S	—
20π	2π	0.10	0.04780	0	0	U	1030
20π	2π	0.10	0.04780	10^{-5}	2.31×10^{-3}	U	1100
20π	2π	0.10	0.04780	10^{-4}	2.31×10^{-2}	S	—
20π	2π	0.12	0.04780	0	0	U	460
20π	2π	0.12	0.04780	10^{-4}	2.31×10^{-2}	U	830
20π	2π	0.12	0.04780	10^{-3}	2.31×10^{-1}	S	—
40π	4π	0.12	0.04909	0	0	S	—

Note: All simulations use $r_h = 1.0$. The column headings are the same as used in Table I. Here the variable n_u refers to first time step where a solution of $\mathbf{Ax} = \mathbf{b}$ exceeds 200 iterations.

water, however, and was not detected in the local analysis. Further investigation of Tables II and III confirms an important trend—the non-linear stability properties of the rotational formulation deteriorate with increasing $k_N h$, whereas for the irrotational formulation the stability properties actually improve! This was also suggested in Section 6.3. This is quite significant, as many of the practical applications of this model involve highly non-linear waves in deep water.

It can be seen from the experiments that the necessary values for the diffusion coefficient D are typically $O(10^{-5})$–$O(10^{-3})\mathrm{m}^2/\mathrm{s}$. These are often somewhat lower than the values $O(10^{-4})$ –$O(10^{-3})\,\mathrm{m}^2/\mathrm{s}$ that might be inferred from the local non-linear analysis in Section 6. This discrepancy is likely, at least in part, due to the dissipative nature of these simulations. The diffusive terms inevitably result in an energy loss, thus the waveheight (and correspondingly the degree of non-linearity) continually decreases during a simulation. This occurs quite rapidly e.g. with $D = 10^{-3}\ \mathrm{m}^2/\mathrm{s}$, effectively making it impossible to test the performance of high non-linearity combined with larger diffusion coefficients for an extended time period. This discrepancy with the local non-linear analysis is not of great concern, given that the original intent was to gain qualitative knowledge for this system. Note also that these necessary values for D are one to three orders of magnitude larger than the kinematic viscosity of water $\nu \approx 10^{-6}\,\mathrm{m}^2/\mathrm{s}$. Thus, the numerical dissipation required for numerical stability is in most cases significantly greater than what might be included for purely physical reasons. The resulting values for r_p are in all cases significantly lower (typically by orders of magnitude) than the corresponding stability limit, perhaps making this limit of little practical significance (at least for this particular time stepping scheme).

The general numerical stability for this non-linear system is an extremely complicated issue, and a full account has certainly not been presented here. These results should, however, provide useful guidelines for future applications of the non-linear model for the general study of water waves.

9. CONCLUSIONS

This paper investigates the numerical stability of method of lines discretizations of the high-order Boussinesq formulation of References [1, 2] for the study of highly non-linear and extremely dispersive water waves. It is shown through linear analyses that centred finite difference schemes are conditionally stable for time stepping schemes whose stability regions contain some portion of the imaginary axis. From the results presented here necessary stability criterion can be established for numerous time integration schemes in combination with a number of finite difference spatial discretizations. Linear analyses using conventional Fourier (von Neumann) techniques in a single horizontal dimension and matrix-based methods in two horizontal dimensions (for both rotational and irrotational formulations) give very similar results, with both indicating that the high-order discretizations result in more restrictive stability constraints than do second-order finite difference approximations.

The matrix-based method is also extended to include the local effects of the non-linear terms. The general de-stabilizing effects of these terms are demonstrated, as are the stabilizing effects of numerical dissipation. The analysis provides clear evidence that the numerical model becomes increasingly unstable as the non-linearity becomes stronger. Although the linear analyses show only minor differences between the rotational and irrotational formulations, much more dramatic differences are demonstrated in the local non-linear analysis. Specifically, it is shown (locally) that the eigenvalues from the rotational system are much less receptive to numerical dissipation than are those from the irrotational formulation when high non-linearity is combined with large water depths and/or refined grids (i.e. large $k_{\mathrm{N}}h$). Alternatively, the analysis suggests that the stability properties of the irrotational formulation actually improve with increasing $k_{\mathrm{N}}h$. Computation of matrix pseudospectra shows that the system is generally

only moderately non-normal, giving confidence that the eigenvalues reasonably characterize the discrete systems. Increased non-normality is, however, demonstrated for the rotational formulation when high non-linearity is combined with large $k_N h$, providing yet further evidence of deteriorating stability properties for this formulation in these circumstances.

A series of numerical experiments demonstrates excellent agreement with the linear analyses, and good qualitative agreement with the local non-linear analysis. These experiments provide further insight, indicating that the rotational formulation has slightly better stability properties in highly non-linear shallow-water situations. The experiments confirm that the irrotational formulation has significantly better stability properties in cases having high deep-water non-linearity, particularly with large $k_N h$. From this analysis it can confidently be concluded that the irrotational formulation is preferable from a stability standpoint in these circumstances. The experiments also demonstrate that the non-linear stability properties of the irrotational formulation improve with increasing $k_N h$, consistent with the local non-linear analysis. These conclusions are significant, as many of the practical applications of this model involve highly non-linear waves in deep water.

This work serves as an example of the combined use of many widely applicable numerical analysis techniques, with each providing valuable insight into the numerical behaviour of this complicated system of PDEs (including up to fifth-order spatial derivatives). Extension beyond classical linear methods of analysis has proven essential for the understanding of this system, as the behaviour of the non-linear model deviates significantly from what might be expected from a strictly linear analysis. This work has proven essential in obtaining convergent numerical solutions for this important high-order system of non-linear PDEs.

APPENDIX A: DIFFERENTIAL OPERATORS

This section includes the various operators in the system of PDEs denoted herein as $\mathscr{A}$. The enhanced free surface operators from rotational (11) and irrotational (13) systems are

$$\mathscr{A}_{11} = 1 - \alpha_2 \left(\frac{\partial^2}{\partial x^2} \right) + \alpha_4 \left(\frac{\partial^4}{\partial x^4} + \frac{\partial^4}{\partial x^2 \partial y^2} \right) \tag{A1}$$

$$\mathscr{A}_2 = -\alpha_2 \left(\frac{\partial^2}{\partial x \partial y} \right) + \alpha_4 \left(\frac{\partial^4}{\partial x^3 \partial y} + \frac{\partial^4}{\partial x \partial y^3} \right) \tag{A2}$$

$$\mathscr{B}_{11} = (\eta - \hat{z}) \left(\frac{\partial}{\partial x} \right) - \beta_3 \left(\frac{\partial^3}{\partial x^3} + \frac{\partial^3}{\partial x \partial y^2} \right) + \beta_5 \left(\frac{\partial^5}{\partial x^5} + 2 \frac{\partial^5}{\partial x^3 \partial y^2} + \frac{\partial^5}{\partial x \partial y^4} \right) \tag{A3}$$

$$\mathscr{A}_{22} = 1 - \alpha_2 \left(\frac{\partial^2}{\partial y^2} \right) + \alpha_4 \left(\frac{\partial^4}{\partial x^2 \partial y^2} + \frac{\partial^4}{\partial y^4} \right) \tag{A4}$$

$$\mathscr{B}_{12} = (\eta - \hat{z}) \left(\frac{\partial}{\partial y} \right) - \beta_3 \left(\frac{\partial^3}{\partial x^2 \partial y} + \frac{\partial^3}{\partial y^3} \right) + \beta_5 \left(\frac{\partial^5}{\partial x^4 \partial y} + 2 \frac{\partial^5}{\partial x^2 \partial y^3} + \frac{\partial^5}{\partial y^5} \right) \tag{A5}$$

$$\mathscr{A}_1 = 1 - \alpha_2 \left(\frac{\partial^2}{\partial x^2} + \frac{\partial^2}{\partial y^2} \right) + \alpha_4 \left(\frac{\partial^4}{\partial x^4} + 2 \frac{\partial^4}{\partial x^2 \partial y^2} + \frac{\partial^4}{\partial y^4} \right) \tag{A6}$$

with the α and β coefficients in (9) applied at $z=\eta$ for the non-linear system and at $z=0$ for the linearized system. The basic bottom operators are

$$\mathscr{A}_{01} = (h+\hat{z})\left(\frac{\partial}{\partial x}\right) - \frac{1}{9}(h+\hat{z})^3\left(\frac{\partial^3}{\partial x^3} + \frac{\partial^3}{\partial x \partial y^2}\right) + \frac{1}{945}(h+\hat{z})^5\left(\frac{\partial^5}{\partial x^5} + 2\frac{\partial^5}{\partial x^3 \partial y^2} + \frac{\partial^5}{\partial x \partial y^4}\right) \tag{A7}$$

$$\mathscr{A}_{02} = (h+\hat{z})\left(\frac{\partial}{\partial y}\right) - \frac{1}{9}(h+\hat{z})^3\left(\frac{\partial^3}{\partial x^2 \partial y} + \frac{\partial^3}{\partial y^3}\right) + \frac{1}{945}(h+\hat{z})^5\left(\frac{\partial^5}{\partial x^4 \partial y} + 2\frac{\partial^5}{\partial x^2 \partial y^3} + \frac{\partial^5}{\partial y^5}\right) \tag{A8}$$

$$\mathscr{B}_0 = 1 - \frac{4}{9}(h+\hat{z})^2\left(\frac{\partial^2}{\partial x^2} + \frac{\partial^2}{\partial y^2}\right) + \frac{1}{63}(h+\hat{z})^4\left(\frac{\partial^4}{\partial x^4} + 2\frac{\partial^4}{\partial x^2 \partial y^2} + \frac{\partial^4}{\partial y^4}\right) \tag{A9}$$

Note that the complete system of operators for both formulations (including variable bottom terms) can be found in Reference [3].

APPENDIX B: THE JACOBIAN MATRIX

This appendix provides a complete description for the computation of the individual components of the Jacobian matrix from (35), which is used in the local non-linear stability analysis in Section 6. Direct differentiation of (1)–(3) as implied by the elements in (35) leads to

$$\frac{\partial}{\partial \eta}\left(\frac{\partial \eta}{\partial t}\right) = -\tilde{U}\frac{\partial}{\partial x} - \tilde{V}\frac{\partial}{\partial y} + 2\tilde{w}\left(\frac{\partial \eta}{\partial x}\frac{\partial}{\partial x} + \frac{\partial \eta}{\partial y}\frac{\partial}{\partial y}\right) + D\nabla^2 \tag{B1}$$

$$\frac{\partial}{\partial \tilde{U}}\left(\frac{\partial \eta}{\partial t}\right) = -\frac{\partial \eta}{\partial x} + \left(1 + \left(\frac{\partial \eta}{\partial x}\right)^2 + \left(\frac{\partial \eta}{\partial y}\right)^2\right)\frac{\partial \tilde{w}}{\partial \tilde{U}} \tag{B2}$$

$$\frac{\partial}{\partial \tilde{V}}\left(\frac{\partial \eta}{\partial t}\right) = -\frac{\partial \eta}{\partial y} + \left(1 + \left(\frac{\partial \eta}{\partial x}\right)^2 + \left(\frac{\partial \eta}{\partial y}\right)^2\right)\frac{\partial \tilde{w}}{\partial \tilde{V}} \tag{B3}$$

$$\frac{\partial}{\partial \eta}\left(\frac{\partial \tilde{U}}{\partial t}\right) = -g\frac{\partial}{\partial x} + 2\tilde{w}\frac{\partial \tilde{w}}{\partial x}\left(\frac{\partial \eta}{\partial x}\frac{\partial}{\partial x} + \frac{\partial \eta}{\partial y}\frac{\partial}{\partial y}\right) + \tilde{w}^2\left(\frac{\partial^2 \eta}{\partial x \partial y}\frac{\partial}{\partial y} + \frac{\partial \eta}{\partial y}\frac{\partial^2}{\partial x \partial y} + \frac{\partial^2 \eta}{\partial x^2}\frac{\partial}{\partial x} + \frac{\partial \eta}{\partial x}\frac{\partial^2}{\partial x^2}\right) \tag{B4}$$

$$\frac{\partial}{\partial \tilde{U}}\left(\frac{\partial \tilde{U}}{\partial t}\right) = -\frac{\partial \tilde{U}}{\partial x} - \tilde{U}\frac{\partial}{\partial x} + \left(1 + \left(\frac{\partial \eta}{\partial x}\right)^2 + \left(\frac{\partial \eta}{\partial y}\right)^2\right)\left(\frac{\partial \tilde{w}}{\partial x}\frac{\partial \tilde{w}}{\partial \tilde{U}} + \tilde{w}\frac{\partial}{\partial \tilde{U}}\left(\frac{\partial \tilde{w}}{\partial x}\right)\right) + 2\tilde{w}\left(\frac{\partial \eta}{\partial y}\frac{\partial^2 \eta}{\partial x \partial y} + \frac{\partial \eta}{\partial x}\frac{\partial^2 \eta}{\partial x^2}\right)\frac{\partial \tilde{w}}{\partial \tilde{U}} + D\nabla^2 \tag{B5}$$

$$\frac{\partial}{\partial \tilde{V}}\left(\frac{\partial \tilde{U}}{\partial t}\right) = -\frac{\partial \tilde{V}}{\partial x} - \tilde{V}\frac{\partial}{\partial x} + \left(1 + \left(\frac{\partial \eta}{\partial x}\right)^2 + \left(\frac{\partial \eta}{\partial y}\right)^2\right)\left(\frac{\partial \tilde{w}}{\partial x}\frac{\partial \tilde{w}}{\partial \tilde{V}} + \tilde{w}\frac{\partial}{\partial \tilde{V}}\left(\frac{\partial \tilde{w}}{\partial x}\right)\right) + 2\tilde{w}\left(\frac{\partial \eta}{\partial y}\frac{\partial^2 \eta}{\partial x \partial y} + \frac{\partial \eta}{\partial x}\frac{\partial^2 \eta}{\partial x^2}\right)\frac{\partial \tilde{w}}{\partial \tilde{V}} \tag{B6}$$

$$\frac{\partial}{\partial \eta}\left(\frac{\partial \tilde{V}}{\partial t}\right) = -g\frac{\partial}{\partial y} + 2\tilde{w}\frac{\partial \tilde{w}}{\partial y}\left(\frac{\partial \eta}{\partial x}\frac{\partial}{\partial x} + \frac{\partial \eta}{\partial y}\frac{\partial}{\partial y}\right) + \tilde{w}^2\left(\frac{\partial^2 \eta}{\partial y^2}\frac{\partial}{\partial y} + \frac{\partial \eta}{\partial y}\frac{\partial^2}{\partial y^2} + \frac{\partial^2 \eta}{\partial x \partial y}\frac{\partial}{\partial x} + \frac{\partial \eta}{\partial x}\frac{\partial^2}{\partial x \partial y}\right) \tag{B7}$$

$$\frac{\partial}{\partial \tilde{U}}\left(\frac{\partial \tilde{V}}{\partial t}\right) = -\frac{\partial \tilde{U}}{\partial y} - \tilde{U}\frac{\partial}{\partial y} + \left(1 + \left(\frac{\partial \eta}{\partial x}\right)^2 + \left(\frac{\partial \eta}{\partial y}\right)^2\right)\left(\frac{\partial \tilde{w}}{\partial y}\frac{\partial \tilde{w}}{\partial \tilde{U}} + \tilde{w}\frac{\partial}{\partial \tilde{U}}\left(\frac{\partial \tilde{w}}{\partial y}\right)\right) + 2\tilde{w}\left(\frac{\partial \eta}{\partial y}\frac{\partial^2 \eta}{\partial y^2} + \frac{\partial \eta}{\partial x}\frac{\partial^2 \eta}{\partial x \partial y}\right)\frac{\partial \tilde{w}}{\partial \tilde{U}} \tag{B8}$$

$$\frac{\partial}{\partial \tilde{V}}\left(\frac{\partial \tilde{V}}{\partial t}\right) = -\frac{\partial \tilde{V}}{\partial y} - \tilde{V}\frac{\partial}{\partial y} + \left(1 + \left(\frac{\partial \eta}{\partial x}\right)^2 + \left(\frac{\partial \eta}{\partial y}\right)^2\right)\left(\frac{\partial \tilde{w}}{\partial y}\frac{\partial \tilde{w}}{\partial \tilde{V}} + \tilde{w}\frac{\partial}{\partial \tilde{V}}\left(\frac{\partial \tilde{w}}{\partial y}\right)\right) + 2\tilde{w}\left(\frac{\partial \eta}{\partial y}\frac{\partial^2 \eta}{\partial y^2} + \frac{\partial \eta}{\partial x}\frac{\partial^2 \eta}{\partial x \partial y}\right)\frac{\partial \tilde{w}}{\partial \tilde{V}} + D\nabla^2 \tag{B9}$$

where (similar to Section 5)

$$\tilde{w} = \mathscr{A}_1\mathscr{Z}_{31}\tilde{U} + \mathscr{A}_1\mathscr{Z}_{32}\tilde{V} - \mathscr{B}_{11}\mathscr{Z}_{11}\tilde{U} - \mathscr{B}_{11}\mathscr{Z}_{12}\tilde{V} - \mathscr{B}_{12}\mathscr{Z}_{21}\tilde{U} - \mathscr{B}_{12}\mathscr{Z}_{22}\tilde{V} \tag{B10}$$

$$\frac{\partial \tilde{w}}{\partial \tilde{U}} = \mathscr{A}_1\mathscr{Z}_{31} - \mathscr{B}_{11}\mathscr{Z}_{11} - \mathscr{B}_{12}\mathscr{Z}_{21} \tag{B11}$$

$$\frac{\partial \tilde{w}}{\partial \tilde{V}} = \mathscr{A}_1\mathscr{Z}_{32} - \mathscr{B}_{11}\mathscr{Z}_{12} - \mathscr{B}_{12}\mathscr{Z}_{22} \tag{B12}$$

Note that while η is included (via the operators $\mathscr{A}_i$, $\mathscr{B}_i$, and $\mathscr{Z}_i$) in the local determination for $\tilde{w}$ in (B10), there are formally $\partial\tilde{w}/\partial\eta$ terms missing in (B1), (B4), and (B7). The neglect

of these terms is justified by the weak dependence of the operators on η (particularly in deep water), and by the extreme complexity of doing otherwise.

Finally, it is again implied that to form the actual Jacobian matrix **J** the continuous operators specified in this appendix must be considered, respectively, in their discrete forms.

ACKNOWLEDGEMENTS

The authors would like to thank the Numerical Analysis Group at Oxford University for hosting part of this work. In particular Prof. L. Nick Trefethen is acknowledged for enlightening discussions on the matrix-based approach and in the interpretation of the pseudospectra computations. Dr Thomas Wright is also acknowledged for helpful discussions on the use of the EigTool software package. This work was financed by the Danish Technical Research Council (STVF Grant No. 9801635). Their support is greatly appreciated. We finally thank the Danish Center for Scientific Computing for providing supercomputing resources.

REFERENCES

1. Madsen PA, Bingham HB, Liu H. A new Boussinesq method for fully nonlinear waves from shallow to deep water. *Journal of Fluid Mechanics* 2002; **462**:1–30.
2. Madsen PA, Bingham HB, Schäffer HA. Boussinesq-type formulations for fully nonlinear and extremely dispersive water waves: derivation and analysis. *Proc. R. Soc. Lond. A* 2003; **459**:1075–1104.
3. Fuhrman DR, Bingham HB. Numerical solutions of fully non-linear and highly dispersive Boussinesq equations in two horizontal dimensions. *International Journal for Numerical Methods in Fluids* 2004; **44**:231–255.
4. Zakharov VE. Stability of periodic waves of finite amplitude on the surface of a deep fluid. *J. Appl. Mech. Tech. Phys.* 1968; **9**:190–194.
5. Madsen PA, Agnon Y. Accuracy and convergence of velocity formulations for water waves in the framework of Boussinesq theory. *Journal of Fluid Mechanics* 2003; **477**:285–319.
6. Madsen PA, Schäffer HA. A review of Boussinesq-type equations for gravity waves. In *Advances in Coastal and Ocean Engineering*, vol. 5, Liu P (ed). World Scientific: Singapore, 1999; 1–95.
7. Madsen PA, Fuhrman DR, Wang B. A Boussinesq-type method for fully nonlinear waves interacting with a rapidly varying bathymetry. *Journal of Fluid Mechanics*, submitted.
8. Trefethen LN. *Spectral Methods in Matlab*. SIAM: Philadelphia, PA, 2000.
9. Iserles A. *A First Course in the Numerical Analysis of Differential Equations*. Cambridge University Press: Cambridge, 1996.
10. Trefethen LN. *Finite Difference and Spectral Methods for Ordinary and Partial Differential Equations*. Unpublished text, 1996. Available: http://web.comlab.ox.ac.uk/oucl/work/nick.trefethen/pdetext.html.
11. Hirsch C. *Numerical Computation of Internal and External Flows, vol 1. Fundamentals of Numerical Discretization*. Wiley: New York, 1988.
12. Fornberg B. *A Practical Guide to Pseudospectral Methods*. Cambridge University Press: Cambridge, 1998.
13. Hindmarsh AC. ODEPACK, a systematized collection of ODE solvers. *IMACS Transactions on Scientific Computation* 1983; **1**:55–64.
14. Petzold LR. A description of DDASSL: a differential/algebraic system solver. *IMACS Transactions on Scientific Computation* 1983; **1**:65–68.
15. Šolín P, Segeth K. Application of the method of lines to unsteady compressible Euler equations. *International Journal for Numerical Methods in Fluids* 2003; **41**:519–535.
16. Abbott MB, Minns AW. *Computational Hydraulics* (2nd edn). Ashgate, Brookfield, U.S.A., 1998.
17. Fischer G. A numerical method for tidal computations in inner seas (in German). *Tellus* 1959; **11**:60–76.
18. Van Der Houwen PJ, Mooiman J, Wubs FW. Numerical analysis of time-dependent Boussinesq models. *International Journal for Numerical Methods in Fluids* 1991; **13**:1235–1250.
19. Savitzky A, Golay MJE. Smoothing and differentiation of data by simplified least squares procedures. *Analytical Chemistry* 1964; **36**:1627–1639.
20. Press WH, Teukolsky SA, Vetterling WT, Flannery BP. *Numerical Recipes in FORTRAN: The Art of Scientific Computing* (2nd edn). Cambridge University Press: Cambridge, 1992.
21. Fuhrman DR, Madsen PA, Bingham HB. A numerical study of crescent waves. *Journal of Fluid Mechanics*, (in press).
22. Embree M, Trefethen LN. Pseudospectra Gateway. Web site: http://www.comlab.ox.ac.uk/pseudospectra.
23. Trefethen LN. Pseudospectra of linear operators. *SIAM Review* 1997; **39**:383–406.

24. Trefethen LN, Trefethen AE, Reddy SC, Driscoll TA. Hydrodynamic stability without eigenvalues. *Science* 1993; **261**:578–584.
25. Trefethen AE, Trefethen LN, Schmid PJ. Spectra and pseudospectra for pipe Poiseiulle flow. *Computer Methods in Applied Mechanics and Engineering* 1999; **175**:413–420.
26. Baggett JS, Trefethen LN. Low-dimensional models of subcritical transition to turbulence. *Physics of Fluids* 1997; **9**:1043–1053.
27. Baggett JS, Driscoll TA, Trefethen LN. A mostly linear model of transition to turbulence. *Physics of Fluids* 1995; **7**:833–838.
28. Wright TG, Trefethen LN. Large-scale computation of pseudospectra using ARPACK and EIGS. *SIAM Journal on Scientific Computing* 2001; **23**:591–605.
29. Wright TG. Algorithms and software for pseudospectra. *Ph.D. Thesis*, Numerical Analysis Group, Oxford University, 2002.
30. Saad Y, Schultz MH. GMRES: a generalized minimal residual algorithm for solving nonsymmetric linear systems. *SIAM Journal on Scientific Computing* 1986; **7**:856–869.

